AIAA 80-0454R

Experimental Modeling of Unstalled Supersonic Turbofan Flutter

Ronald E. Riffel*
General Motors Corporation, Indianapolis, Ind.
and
Sanford Fleeter†
Purdue University, West Lafayette, Ind.

This paper describes the experimental techniques and procedures used to extend the current experimental unsteady rectilinear cascade modeling capability to include the relatively low supersonic inlet Mach number, high pressure ratios, and high reduced-frequency values characteristic of the unstalled supersonic flutter of fan stages. In particular, the cascade modeling concepts, the steady and time-variant experimental techniques, fabrication and instrumentation considerations, data acquisition and reduction procedures, and the correlation of the resulting steady and time-variant cascade data with corresponding predictions are presented.

Nomenclature

A/A^* = isentropic local to throat area ratio
C = airfoil chord
C_p = unsteady pressure coefficient, $C_p = P/[\frac{1}{2}\rho U^2(h/C)]$; $C_p = P/(\frac{1}{2}\rho U^2\alpha)$
f = oscillatory frequency, Hz
h = translational amplitude of oscillation
k = reduced frequency ($k = \omega C/2U$)
M = inlet Mach number
N = number of dynamic data points
p = measured unsteady pressure
Q = dynamic pressure
R_c = cascade pressure ratio
U = inlet velocity
α = torsional amplitude of oscillation
β = flow angle
ΔP_s = static pressure rise across blade element
μ = interblade phase angle, deg
ρ = inlet air density
ω = angular frequency ($\omega = 2\pi f$)

Introduction

SUPERSONIC flutter of fan stages is often found to occur at operating conditions for which the mass flow through the stage is independent of back pressure. At these high operating speeds, a region of supersonic unstalled torsional flutter is encountered in the low back pressure region of the operating map. In addition, a region of high back pressure bending flutter exists in the moderate-to-high back pressure region of the map.

Both of the above-noted modes of supersonic flutter are currently under investigation, with most of these studies analytical in nature. The generally used flow model assumes inviscid flow through a fan stage of differential radial height which is developed into a two-dimensional rectilinear cascade. The airfoils are most often assumed to be zero thickness flat plates which are harmonically oscillating in either a torsion or bending mode with a constant interblade vibratory phase angle.

A number of solutions to this basic model involving various mathematical techniques have been developed, as reviewed in Refs. 1 and 2. For the designer to make use of these solutions in a predictive flutter avoidance design system, it is necessary to quantitatively assess the validity of this mathematical model and to extend it to more realistic airfoil configurations. To accomplish this, fundamental two-dimensional aerodynamic cascade data are needed. However, because of the extreme difficulty in both the experimental modeling of supersonic flutter and the acquisition and analysis of the resulting time-variant data, only very limited cascade data currently exist. These data,[3-5] although of significant and permanent value, are limited in that the Mach number is greater and, for the case of torsion, the reduced frequency values lower than those values corresponding to supersonic flutter of the rotor being modeled.

Both steady and time-variant two-dimensional cascade data are necessary to develop an understanding of the fundamental mechanisms as well as to verify and direct the development of valid unstalled supersonic flutter analytical models. To be of maximum value, these data must be obtained in carefully designed experiments which model the significant features of unstalled supersonic flutter. In particular, the airfoil cascade itself must be a valid two-dimensional representation of an appropriate rotor section; the steady-state aerodynamic conditions of the rotor, including the inlet Mach number and the static pressure ratio values, must be properly obtained in the cascade; time-variant aerodynamic torsion and translation mode data must be obtained at reduced-frequency values corresponding to those of unstalled supersonic flutter in rotors.

The overall objective of the research described herein is to extend the existing experimental unsteady rectilinear cascade modeling capability to include the relatively low supersonic inlet Mach numbers, high pressure ratios, and high reduced-frequency values characteristic of unstalled supersonic flutter of fan stages. In particular, the cascade modeling concepts, the steady and time-variant experimental techniques, fabrication and instrumentation considerations, data acquisition and reduction procedures, and the correlation of the resulting steady and time-variant cascade data with corresponding predictions are presented.

Two-Dimensional Airfoil Cascade Design

Due to the radius change and area convergence existing in a rotor, but not modeled in a two-dimensional cascade, it is not possible for the cascade to have the same inlet and exit Mach numbers and flow angles as the corresponding rotor. However, a viable two-dimensional cascade representation can be achieved by preserving the critical elements of the rotor section flowfield. In particular, for the case of supersonic

Presented as Paper 80-0454 at the AIAA 11th Aerodynamic Testing Conference, Colorado Springs, Colo., March 18-20, 1980; submitted March 18, 1980; revision received Dec. 2, 1980.

*Senior Research Engineer, Detroit Diesel Allison Division. Member AIAA.
†Associate Professor, School of Mechanical Engineering. Member AIAA.

inlet rotor blade sections, the flowfield is critically affected by the shock-wave pattern and, to a much lesser degree, by the specific blade geometry. To preserve this shock pattern, the two-dimensional cascade must maintain the corresponding rotor element values of the following key parameters: the inlet and exit Mach numbers; the critical inlet area ratio, A/A^*; and the rotor critical incidence angle, which is defined as the angle between the upstream air angle and the blade suction surface angle at a point midway between the leading edge and the intersection of the first covered characteristic with the suction surface, as schematically depicted in Fig. 1.

A set of vector diagrams must be produced for the cascade. This is accomplished by preserving the rotor element values for the inlet and exit relative Mach numbers, as noted above, and by setting β_∞ of the cascade equal to the relative β_∞ of the rotor blade element where:

$$\beta_\infty = \tan^{-1}(\tan\beta_1 + \tan\beta_2 / 2)$$

In addition, the stagger angle is also maintained in the cascade in order to preserve the axial velocity component. The design philosophy of the rotor is then applied to define the cascade airfoil profiles. In this procedure, the critical incidence and the critical inlet area ratio are maintained, as are the deviation criteria and such blading parameters as the thickness-to-chord distribution, the maximum thickness, the solidity, and the leading-edge radius-to-chord ratio.

The above-described design procedure results in cascades that are representative of rotor flowfields in terms of Mach number levels, shock locations, and loading distributions, even though the cascade is not a geometrical scale of the rotor blade element. It should be noted that the cascade and rotor do not have identical inlet and exit flow and metal angles and large percentage differences may exist in the overall camber and surface curvature. However, for the class of airfoils of interest for the supersonic inlet Mach number regime, both the total turning and curvature are small. Hence they are not dominant in establishing the character of either the inviscid or boundary-layer flowfields. Table 1 illustrates this cascade design procedure by presenting a comparison of the fundamental parameters for a rotor blade element and the resulting two-dimensional cascade.

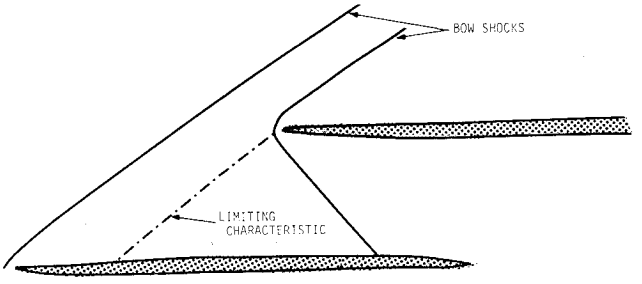

Fig. 1 Blade element inlet flowfield schematic.

Experimental Facility

The flow regime of interest with regard to unstalled supersonic flutter involves inlet Mach numbers on the order of 1.3 and static pressure ratios in the approximate range of 1.0-1.4:1. Careful consideration of the test section configuration is necessary to achieve these relatively low supersonic inlet Mach numbers and high static pressure ratios in a valid two-dimensional rectilinear periodic cascade.

Table 1 Example rotor blade section—airfoil cascade design

	Rotor	Cascade
Velocity diagram data		
Inlet Mach No.	1.213	1.214
Exit Mach No.	0.905	0.905
Inlet air angle, deg	64.95	64.51
Exit air angle, deg	62.81	63.28
Diffusion factor	0.300	0.299
$\Delta P_s/Q$	0.240	0.241
Turning	2.14	1.23
Blading design data		
Inlet metal angle, deg	60.69	60.46
Exit metal angle, deg	61.29	61.76
Inflection angle, deg	62.32	62.70
Net camber, deg	−0.60	−1.30
Forward camber, deg	−1.63	−2.24
Rear camber, deg	+1.03	0.94
Meanline incidence, deg	4.26	4.05
Suction surface incidence, deg	1.60	1.57
Meanline deviation, deg	1.52	1.52
Setting angle, deg	61.57	61.75
Solidity	1.17	1.17
Chord, in.	3.898	3.000
Thickness/chord ratio	0.034	0.034
LER/chord ratio	0.0026	0.0026
TER/chord ratio	0.0026	0.0026
T max location	0.50	0.50
Inflection location	0.769	0.769
Minimum A/A^*	1.030	1.030
β_∞, deg	63.92	63.92

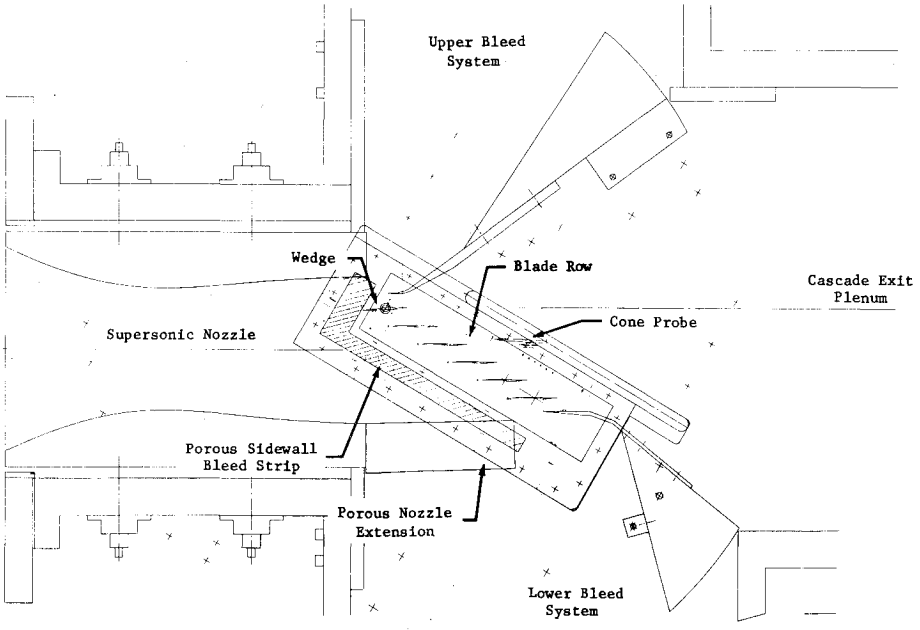

Fig. 2 Schematic of rectilinear cascade wind tunnel.

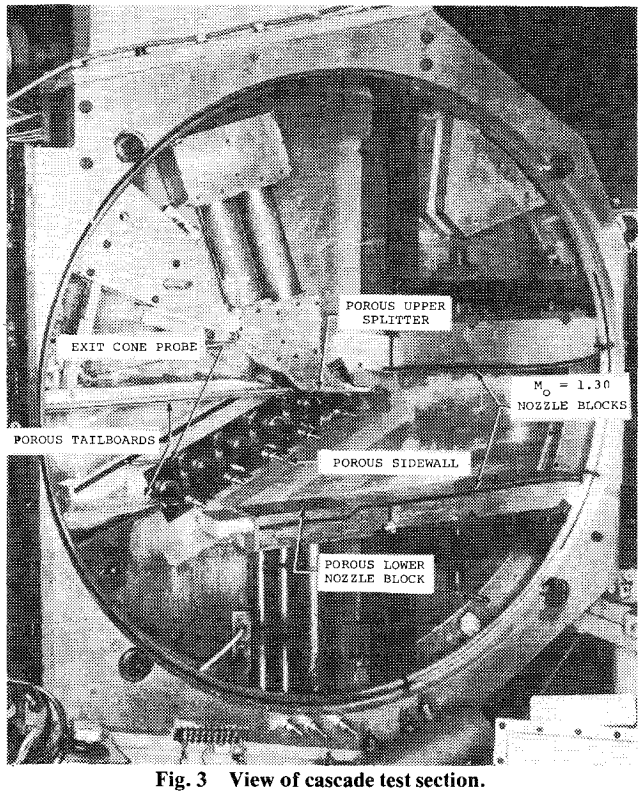

Fig. 3 View of cascade test section.

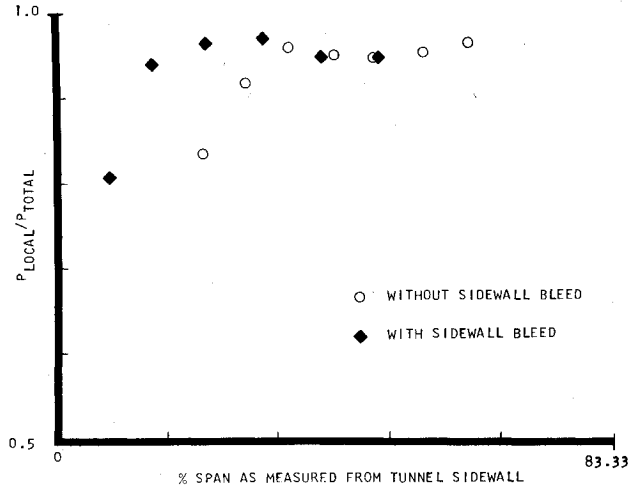

Fig. 4 Effect of sidewall bleed on cascade exit spanwise total pressure distribution.

Table 2 Rotor and corresponding cascade flutter point data

	Frequency,[a] Hz	Inlet relative Mach number (75% span)	Reduced frequency based on 75% span
Rotor A	745 (T)	1.25	0.52
Cascade A	836 (T)	1.25	0.52[b]
Rotor B	440 (B)	1.25	0.16
Cascade B	264 (B)	1.25	0.16[b]

[a] T: torsion mode, B: bending mode.
[b] Based on 3.00 in. (7.62 cm) chord.

Figures 2 and 3 show the test section of the Detroit Diesel Allison rectilinear cascade facility. As can be seen, the entrance flow to the test section is generated by fixed nozzle blocks yielding a Mach number of 1.30. The orientation of a wedge with respect to this nozzle exit flow specified the test section Mach number, i.e., the shock or expansion wave generated by the wedge determines the cascade inlet conditions. The cascade inlet flow direction is determined by the orientation of the wedge with respect to the airfoil cascade.

To aid in the establishment of the cascade inlet periodicity, bleed chambers are provided on the lower nozzle block, as indicated. Adjustment of the bleed rate through these chambers allows the inlet flow to the rear (bottom) portion of the cascade to be affected. The inlet flow to the front (upper) portion of the cascade is affected only by the wedge position, with the first passage controlled to some extent by the splitter position. The buildup of the boundary layer in this first passage can produce area ratios such that this passage cannot be started. Hence, suction is provided along the front portion of the splitter to remove the boundary layer and start this first passage.

Active cascade inlet sidewall boundary-layer control is also provided to assure the two-dimensionality of the cascade flowfield. This is accomplished with the porous sidewall bleed strip shown in Fig. 2. It contains five discrete regions yet still permits the Schlieren system to be utilized to view the cascade wave system. The effectiveness of this sidewall bleed system is clearly demonstrated in Fig. 4 which presents the results of spanwise cascade exit total pressure surveys with and without bleed.

Disturbances generated at the lower endwall per the geometry of Figs. 2 and 3 run downstream of the cascade in the supersonic flow regime and thus can have no influence on the cascade performance. The upper endwall of this tunnel, however, is crucial in that it can influence the whole flowfield downstream of the cascade and prevent the formation of a periodic exit flowfield. The shape of this upper endwall also uniquely determines the cascade pressure ratio under started supersonic exit operating conditions. The most crucial portion of the upper endwall is in the early stage of compression. Here the flow splitter provides the capability to both bleed and blow. This capability, in conjunction with adjustments of the exit plenum pressure and the angle of the tailboard attached to the splitter, permits the setting of the streamline shape in this region and thereby sets the throttle condition to the first two channels of the cascade. The remaining problem is to not allow the cascade shock expansion system which impinges upon this tailboard to reflect back into the cascade. This is accomplished by making this upper tailboard porous with a 50% open area as well as having it open to the exit plenum pressure. This effectively produces a streamline representation of an infinite cascade at the design pressure ratio, as established in the first passage, and results in a periodic exit flowfield.

Cascade Drive Systems and Airfoil Fabrication

To acquire two-dimensional data relevant to unstalled supersonic flutter, not only must the steady-state cascade aerodynamic parameters be representative of those for the rotor, but also the key unsteady parameters. In particular, the cascade must meet the requirement that the harmonic torsion and translation mode oscillations are at a frequency such that the value of the reduced frequency k ($k=\omega C/2U$) is equal to that of flutter for the rotor being modeled. A further requirement is that an essentially two-dimensional motion of the airfoils in the proper mode must be attained. Also, the torsion and translation mode drive systems must be capable of forcing the airfoils at a specified frequency over a complete range of interblade phase angle values.

The velocities necessary to attain specific Mach numbers in the cascade test section can be calculated using isentropic relationships and measured upstream stagnation conditions. In general, for the divergent portion of the tunnel, the static temperature drops as a result of the increasing supersonic flow, resulting in a decreased speed of sound. Since aerodynamically the inlet relative Mach number of the rotor is to be maintained, the cascade inlet relative velocity will be

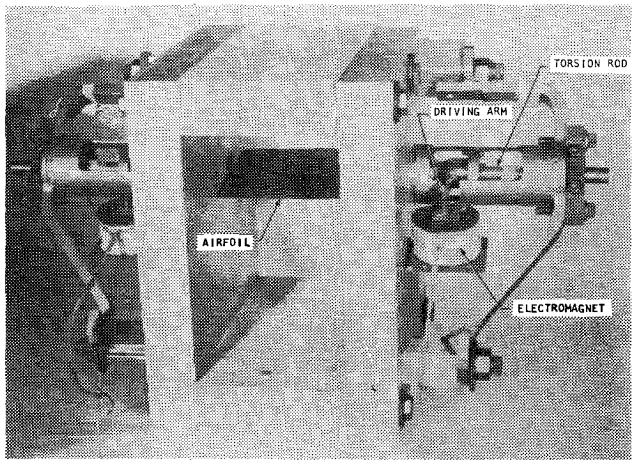

Fig. 5 High-frequency torsion mode drive system bench rig.

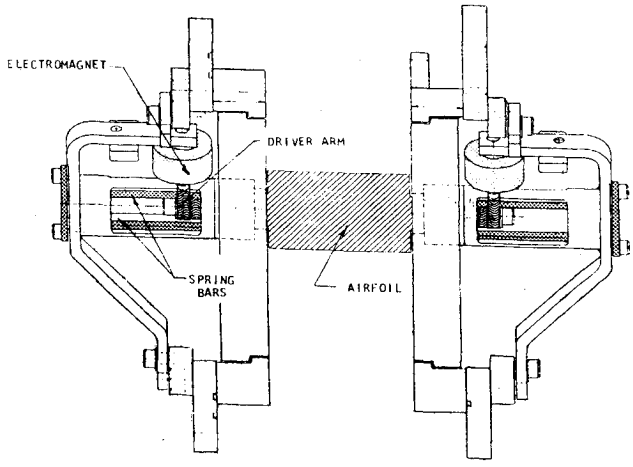

Fig. 6 Schematic of translation mode drive system.

lower than the rotor value because of the lower static temperature. Also, the rotor and cascade blade chord lengths are different because of design considerations in the cascade test section. These velocity and chord changes must be considered when the cascade test frequencies are established. Table 2 lists the values for the flutter frequency and corresponding Mach number for two rotors, one fluttering in a torsional mode and the other in bending (translation). Also listed are the values of the inlet Mach number and frequency of oscillation which must be obtained in the cascade.

A view of the bench rig high-frequency torsion mode airfoil cascade drive system is shown in Fig. 5 and a schematic of the translation mode system in Fig. 6. In both systems the airfoils are positioned with two flexible mounts consisting of a female spline which connects to the corresponding spline on the airfoil trunnion by indexing over six grooves and attaching through a replaceable spring bar in the translation drive system and a torsion rod in the torsion mode system. The airfoil trunnion splines are positioned axially on these devices by a driver arm clamped and piloted to the trunnion with an attached spacer tube which nests over the indexing tabs of the female spline. Excitation forces to each blade are supplied through the drive arm by electromagnets. These electromagnets are computer controlled, thereby permitting arbitrary interblade phase angles to be obtained, as per Refs. 6 and 7. Driving mechanisms are located on each airfoil trunnion so that proper excitation of the two-dimensional translational motion of the airfoil can be accomplished. Modification of the spring bars and/or mass control of the driver arm can be used for minor frequency adjustments of individual blades.

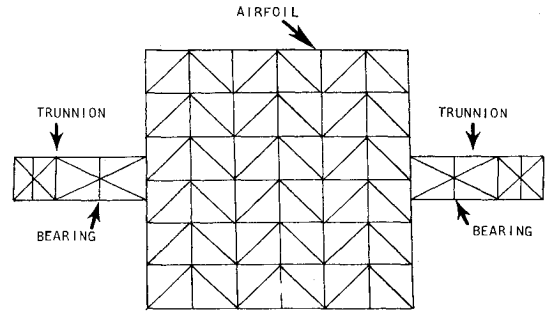

Fig. 7 Top view of finite-element model airfoil.

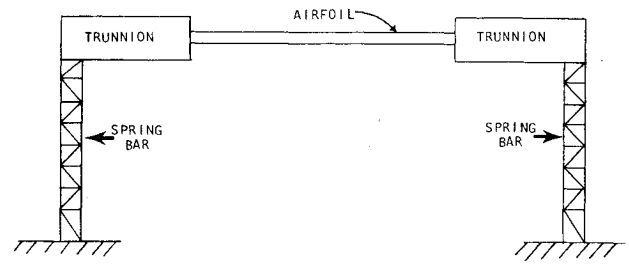

Fig. 8 Frontal view of finite-element model torsion mode drive system.

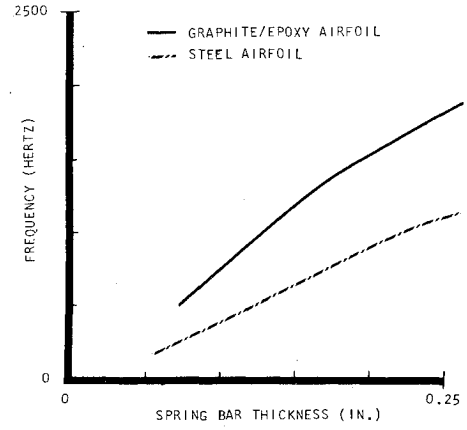

Fig. 9 First torsional mode frequency vs spring bar thickness.

The double-trunnion airfoils and drive system assemblies are mounted in Plexiglas windows, thereby permitting Schlieren flow visualization, and this complete assembly is then installed in the test section. Strain gages mounted on the spring bars or torsion rods exhibit excellent sensitivity to the translational and torsional airfoil oscillations, respectively, and allow the measured strain signals to be converted to amplitudes of oscillation.

Dynamic finite-element analysis of idealized torsion and translation mode cascade drive systems was conducted to determine the required drive system spring constants and to reduce the system inertia so as to minimize the required electromagnetic driving power. Figures 7 and 8 show views of the finite-element airfoil and torsion mode drive system models, respectively. The airfoil chord and span are both 3.00 in. (7.62 cm) and the trunnions are represented by a 0.5 in. (1.27 cm) square bar. Both a steel airfoil and a graphite/epoxy composite airfoil were investigated. Boundary conditions at the bearing location were established such that the airfoil could rotate but not translate.

Using this model, the trend of torsional frequency with increasing spring bar thickness was established for both the steel and composite airfoils with the results presented in Fig. 9. As indicated, significantly thinner spring bars are required to achieve a specified system natural frequency for the

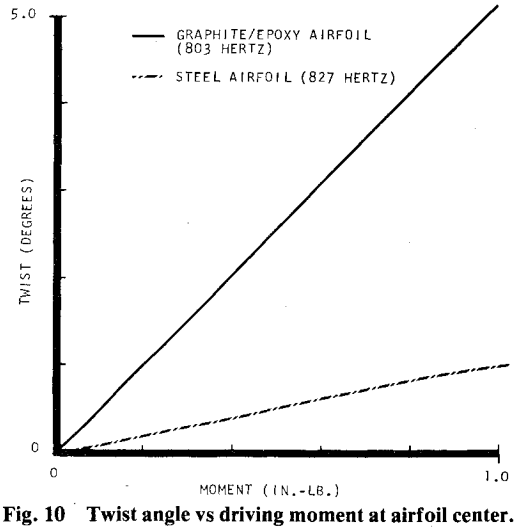

Fig. 10 Twist angle vs driving moment at airfoil center.

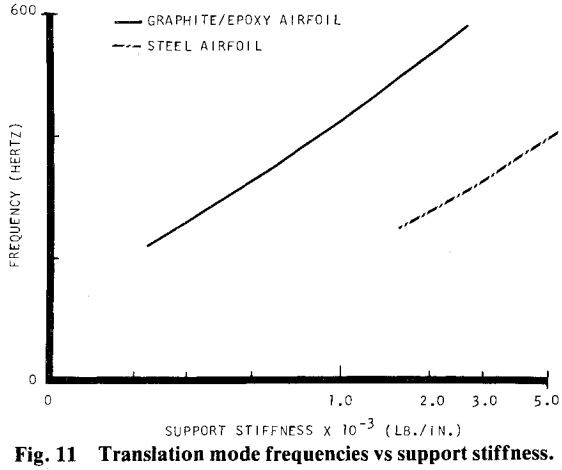

Fig. 11 Translation mode frequencies vs support stiffness.

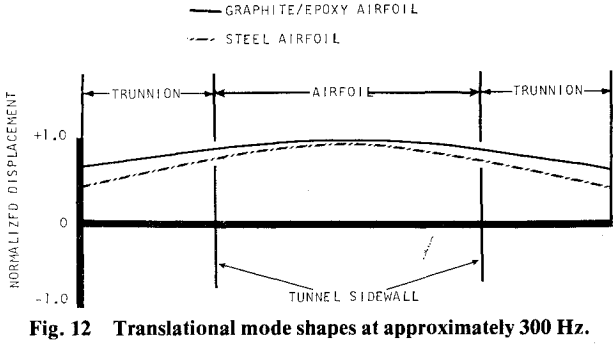

Fig. 12 Translational mode shapes at approximately 300 Hz.

graphite/epoxy composite airfoil than for the steel airfoil, thereby substantially reducing the required electromagnetic airfoil driving force.

To quantify the moment necessary to vibrate the airfoil, a forced response analysis was also performed. A moment of ±1 in.-lb was assumed to be the driving mechanism acting at the spring bar spanwise centerline simultaneously on both trunnions with a structural damping value of 0.01, based on previous cascade experience. To achieve ±0.5 deg of torsional motion at the center of the airfoil, Fig. 10 indicates that input moments at both driving points of ±0.5 in.-lb are required for the steel airfoil and of only ±0.1 in.-lb for the graphite/epoxy composite airfoil.

A similar analysis was also performed for an analogous idealized translation mode drive system. As seen in Fig. 11, which presents the translation mode frequency of the steel and graphite/epoxy composite airfoils as a function of support

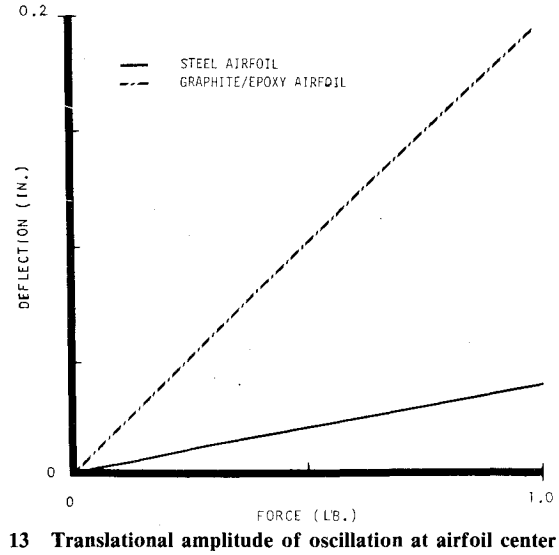

Fig. 13 Translational amplitude of oscillation at airfoil center as a function of input force.

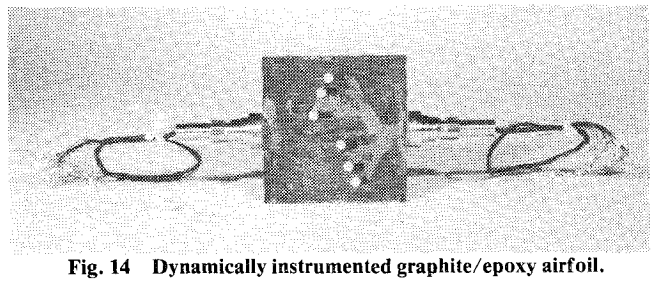

Fig. 14 Dynamically instrumented graphite/epoxy airfoil.

stiffness, less stiffness (a softer system) is again required for the graphite/epoxy composite airfoil. A comparison of the mode shapes for the two airfoils at approximately 300 Hz is presented in Fig. 12. As seen, the graphite/epoxy composite blade is seen to result in nearly rigid body translation across the tunnel, whereas the steel blade exhibits spanwise bending. This is significant in that the cascade airfoils must exhibit rigid body motion to insure the two-dimensionality of the experiment. The results of the forced response analysis demonstrate that significantly less driving force is required for the graphite/epoxy composite airfoil than for the steel airfoil, as presented in Fig. 13.

Thus, as determined by the above-described model torsion and translation mode drive systems, airfoils fabricated from graphite/epoxy composite material are seen to offer many significant advantages over steel airfoils. Hence, cascade airfoils were fabricated from a combination of preimpregnated Kevlar cloth and graphite mat injected with epoxy resin under pressure into a booking mold. Cloth fiber orientation was controlled to meet prescribed torsional and bending stress requirements while maintaining a low density and a high modulus of elasticity.

Hollow steel trunnions were attached to the airfoils at midchord. Cloth insertion and epoxy fill into the trunnions provided adequate strength at the critical airfoil/trunnion interface stress locations. Splines located on the trunnions are used to mount the airfoils into either of the drive systems.

The fabrication of the airfoils from graphite/epoxy composite material necessitated the use of nonconventional instrumentation techniques. In particular, to maintain the desired overall composite material properties with no degradation of the airfoil surface contours, provisions for dynamic instrumentation were embedded in one airfoil during fabrication. This involved molding the dynamic pressure transducer lead wires into the airfoil as part of the lay-up and molding process. The ends of the lead wires were then exposed

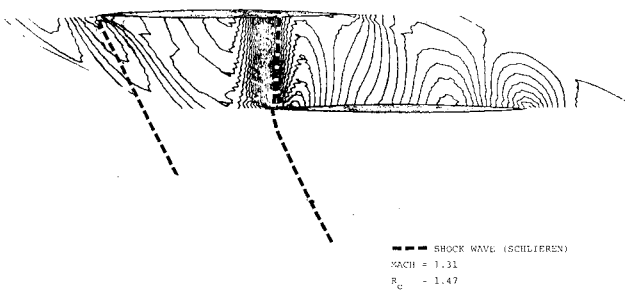

Fig. 15 Comparison of experimental and predicted overall cascade flowfield.

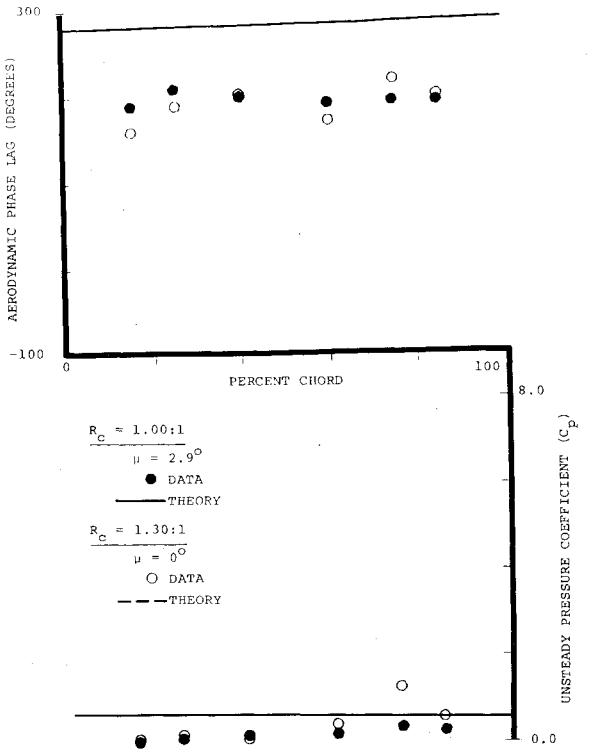

Fig. 16 Unsteady cascade translation mode results on the suction surface.

and the transducers attached. These flush-mounted Kulite dynamic pressure transducers were staggered across the span of the airfoil on both the pressure and suction surfaces. Figure 14 shows a view of one of these unique dynamically instrumented airfoils. The chordwise distribution of these transducers is identical on the airfoil pressure and suction surfaces.

Data Acquisition and Analysis

With the tunnel in operation and the steady-state cascade periodicity properly established, the computer-controlled drive system is made operational. This results in controlled harmonic oscillations of the airfoil cascade at a prescribed frequency and interblade phase angle value. The resulting time-variant spring-bar-mounted strain gage and airfoil surface pressure transducer signals are digitized at rates to 100,000 points/s by a 16-channel analog-digital converter and multiplexer system, and stored on a magnetic disk. These digitized data are analyzed on-line to determine the fundamental aerodynamic characteristics of the unsteady phenomena. The parameters of interest include the amplitude of the airfoil motion and the pressure disturbance, the frequency, the interblade phase angle, and the phase difference between the unsteady pressures and the airfoil motion as characterized by the strain gage signal on the dynamically

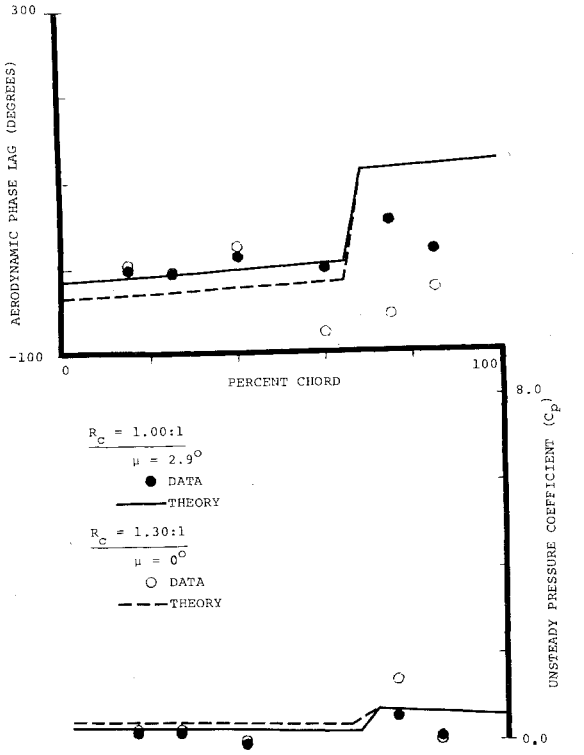

Fig. 17 Unsteady cascade translation mode results on the pressure surface.

instrumented airfoil, i.e., the aerodynamic phase lag data is referenced to the motion of the dynamically instrumented center airfoil in the cascade.

The amplitude of the airfoil motion and the pressure disturbance are determined by fitting a second-order least-square function to the harmonic data, diferentiating it, and evaluating the maximum. The pressure disturbance amplitude is then nondimensionalized into an unsteady pressure coefficient C_p, as defined in Eq. (1) for translation and Eq. (2) for torsion mode oscillations

$$C_p = \frac{p}{\frac{1}{2}\rho U^2 (h/C)} \tag{1}$$

$$C_p = \frac{p}{\frac{1}{2}\rho U^2 \alpha} \tag{2}$$

where p is the measured unsteady pressure amplitude, ρ the inlet air density, U the inlet velocity, α the torsional amplitude of oscillation, and h/C the ratio of the translational amplitude to the airfoil chord.

Results

The experimental procedures necessary to achieve valid modeling of unstalled supersonic turbofan cascade flutter must include first obtaining a periodic steady-state cascade flowfield. A comparison of the overall cascade steady flowfield, as characterized by the location of the shock waves, with that predicted by the analysis of Ref. 7, is presented in Fig. 15. As can be seen, the correlation between the experimentally determined shock waves and those indicated by the predicted constant pressure lines is excellent.

The time-variant aerodynamic characteristics are determined by harmonically oscillating the airfoil cascade in either a torsional or translational mode at appropriate high reduced-frequency values over a range of interblade phase angles. These unique chordwise pressure and suction surface time-variant pressure data are then analyzed to determine the aerodynamic phase lag as referenced to the motion of the

instrumented airfoil and the magnitude of the unsteady pressure coefficient C_p. To ascertain the validity or to indicate refinements in the state-of-the-art unstalled supersonic flutter analyses, these data are correlated with appropriate predictions.

Figures 16 and 17 present two typical high reduced-frequency ($k=0.21$) translation mode data sets together with the corresponding oscillating flat-plate cascade predictions from Ref. 8 at an inlet Mach number of 1.35 for two levels of loading at approximately a 0 deg interblade phase angle value. These data were obtained on a 3.0 in. chord graphite/epoxy classical airfoil cascade characterized by a flat suction surface and a wedge-shaped pressure surface with a maximum thickness of 0.15 in. at midchord. As indicated, the time-variant suction surface data (Fig. 16) are seen to generally exhibit very good trendwise correlation with the predictions. The aerodynamic phase lag and unsteady pressure coefficient data are both nearly constant in the chordwise direction, with the theory predicting an approximate 60 deg greater lag than that characteristic of the data. As the effects of increased static pressure ratio are largely taken up in the trailing-edge wave system, only the trailing edge of the suction surface should be affected, as is evidenced in Fig. 16.

The time-variant pressure surface data (Fig. 17) also generally exhibit very good correlation with the theoretical predictions. Both the aerodynamic phase lag and the unsteady pressure coefficient data and prediction remain nearly constant in the chordwise direction between the leading edge and the midchord region shock-wave intersection location on this surface. The theory predicts that intersection location to be at approximately 70% of the chord, with the 1.00/1 pressure ratio data indicating the presence of a shock in the region between the 60 and 75% chord transducer locations. Comparison of the 1.00:1 and the 1.30:1 pressure ratio data indicates that the effect of increasing back pressure is to move the shock intersection forward on the pressure surface such that at the higher pressure ratio it lies between the 90 and 60% chord transducer locations.

Summary

This paper has described the experimental techniques and procedures necessary to extend significantly the current experimental unsteady cascade modeling capability to include the relatively low supersonic inlet Mach number, high pressure ratio, and high reduced-frequency values characteristic of unstalled supersonic flutter of fan stages. In particular, the cascade modeling concepts, the steady and time-variant experimental techniques, fabrication and instrumentation considerations, data acquisition and reduction procedures, and the correlation of the steady and high-frequency time-variant translation mode oscillating cascade data with corresponding state-of-the-art predictions have been presented.

References

[1] Chadwick, W.R., Bell, J.K., and Platzer, M.F., "On the Analysis of Supersonic Flow Past Oscillating Cascades," *Unsteady Phenomena in Turbomachinery, AGARD-CP-177,* 1975.

[2] Strada, J.A., Chadwick, W.R., and Platzer, M.F., "Aeroelastic Stability Analysis of Supersonic Cascades," *ASME Journal of Engineering for Power,* Vol. 101, Oct. 1979, pp. 533-541.

[3] Fleeter, S., Novick, A.S., Riffel, R.E., and Caruthers, J.E., "Experimental Determination of the Unsteady Aerodynamics in a Controlled Oscillating Cascade," *ASME Journal of Engineering for Power,* Vol. 99, Jan. 1977.

[4] Fleeter, S. and Riffel, R.E., "Aerodynamic Phenomena in an Oscillating Transonic MCA Airfoil Cascade Including Loading Effects," *NATO-AGARD Conference on Unsteady Aerodynamics,* AGARD-CP-227, Sept. 1977.

[5] Fleeter, S., Riffel, R.E., Lindsey, R.H., and Rothrock, M.D., "A Supersonic Turbofan Cascade in Translation," *NATO-AGARD Conference on Stresses, Vibration, Structural Integration and Engine Integrity,* AGARD-CP-248, Oct. 1978.

[6] Fleeter, S., McClure, R.B., Holtman, R.L., and Sinnet, G.T., "Supersonic Inlet Torsional Cascade Flutter," *Journal of Aircraft,* Vol. 12, 1975, pp.

[7] Delaney, R.A. and Kavanagh, P., "Transonic Flow Analysis in Axial-Flow Turbomachinery Cascades by a Time-Dependent Method of Characteristics," ASME Paper 75-GT-8, 1975.

[8] Caruthers, J.E., "Theoretical Analysis of Unsteady Supersonic Flow Around Harmonically Oscillating Turbofan Cascades," Ph.D. Thesis, Georgia Institute of Technology, Atlanta, Ca., September 1976.